Disorder-driven cluster glass state in a geometrically frustrated hexagonal perovskite

Shruti Chakravarty,[1] Øystein Slagtern Fjellvåg,[2,3] Arpan Bhattacharyya,[4,*] Lukas Keller,[2] and Sunil Nair[1,†]

[1]*Department of Physics, Indian Institute of Science Education and Research, Pune, India*

[2]*Laboratory for Neutron Scattering and Imaging, Paul Scherrer Institut, Villigen CH-5232, Switzerland*

[3]*Department for Hydrogen Technology, Institute for Energy Technology, NO-2027 Kjeller, Norway*

[4]*Saha Institute of Nuclear Physics, 1/AF Bidhannagar, Kolkata, India*

(Received 14 September 2022; revised 3 February 2023; accepted 29 March 2023; published 12 April 2023)

We report the observation of cluster glasslike properties in a double perovskite ruthenate Ba_2CoRuO_6 through structural (neutron and synchrotron x-ray diffraction), magnetic, and transport measurements. The system exhibits classic glassy characteristics such as a frequency dependence in ac susceptibility, aging and memory effects, along with the persistence of short-range correlations up to room temperature. The significant ($\sim$30%) antisite disorder on the dimer sites, coupled with the inherent geometrical frustration, allows a variety of exchange (both antiferro- and ferromagnetic) interactions to be distributed randomly across the lattice. On cooling, locally dominant interactions cause spins to nucleate and form local, short-range ordered clusters which grow in size until a global freezing occurs at about $T_f \sim 43$ K.

DOI: 10.1103/PhysRevB.107.134414

I. INTRODUCTION

Double perovskite oxides of the type $A_2BB'O_6$ have been extensively studied as a fertile arena to probe emergent magnetic and electric phenomena for many years now. Ideally, a double perovskite is generated by substituting exactly half of the B sites with a different cation resulting in a three-dimensional rocksalt order. However, the matching between ionic radii of the A and B cations is crucial towards achieving this perfect order and is parametrized by the Goldschmidt tolerance factor, $t = \frac{r_A + r_O}{\sqrt{2}(\frac{r_B + r_{B'}}{2} + r_O)}$, where r_A, r_B, $r_{B'}$, and r_O are the ionic radii of A, B, B', and O, respectively. When $t < 1$, tilting of the BO_6 octahedra occurs to compensate for the cation mismatch. When $t > 1$ (like for Ba_2CoRuO_6, $t = 1.071$), the strain is too large, tilting is not enough, and face sharing becomes more common [1]. The 6H perovskite structure is most commonly encountered when studying triple perovskite layered systems with the chemical formula $A_3BB'_2O_9$ where the B and B' cations have two crystallographically distinct positions. They contain face-sharing octahedra or dimers where a strong orbital overlap between the B' cations can occur and compete with the intra- and interoctahedra superexchange interactions. In some 6H perovskites, due to the strong hybridization between the B' and O orbitals, the B'_2O_9 dimers are suggested as the relevant "molecular units" instead [2,3]. This debate between whether face-shared dimers can be regarded as molecules with defined molecular orbitals or not, is an inherently fascinating feature of 6H perovskites [4].

The $3d/4d$ combination of B and B' cations is particularly interesting due to the difference in the spatial extent of the $3d$ and $4d$ orbitals as well as the increased importance of spin-orbit coupling in the latter. Ru^{5+} is a particularly intriguing $4d$ ion since it often treads the line between localized and delocalized electron behavior [1] due to both the high correlation energy of the t_{2g}^3 configuration and a wider $4d$ valence band. The freedom to tune the dimers from a localized (superexchange) to the itinerant (direct exchange or metal-metal bonding) limit enables Ru-based perovskites to display a wide array of interesting electronic and magnetic phenomena including orbital/charge order [2]; frustrated, molecular quantum magnets [5]; large zero-field splitting [6]; and orbital selective Mott insulating behavior at the molecular level [7]. Incommensurate magnetic structures [8], glassy dynamics and magnetic frustration [9–11], colossal dielectric constants [12], spin-liquid behavior [13], and even superconductivity [14] has been observed in Ru-based double perovskite systems.

Ba_2CoRuO_6 mimics this 6H structure with a random distribution of Co and Ru within the face-sharing octahedra, and can be written as $Ba_3Co[Co_{0.25}Ru_{0.75}]_2O_9$. Thus, it is evident that Ba_2CoRuO_6 inherently possesses significant site disorder, which gives rise to complex magnetic behavior at low temperature. In an attempt to fully interpret this influence of disorder on the magnetic ground state, we have synthesized this material and extensively characterized it through structural, magnetic, dielectric, thermal and electronic transport, along with temperature dependent neutron and synchrotron measurements.

II. EXPERIMENTAL METHODS

Polycrystalline samples of Ba_2CoRuO_6 were prepared via a solid-state synthesis method using stoichiometric amounts of raw materials ($BaCO_3$, Co_3O_4, and RuO_2) following the procedure detailed in [15]. The raw materials were mixed and ground in a mortar using ethanol until a fine,

*Present address: S. N. Bose National Center for Basic Sciences, JD Block, Salt Lake Sector 3, Kolkata 700106, India.

†Corresponding author: sunil@iiserpune.ac.in

homogeneous mixture was obtained. The mixture was then heated at 1150 °C twice, for 24 h each with intermediate regrinding and pelletization. Laboratory x-ray diffraction (XRD) measurements at room temperature performed using a Bruker D8 Advance diffractometer (Cu $K\alpha$ $\lambda = 1.5406$ Å) confirmed the sample to be pure and single phase. Elemental compositions and their homogeneity were reconfirmed by using an energy dispersive x-ray spectrometer (Ziess Ultra Plus). The average stoichiometry calculated from statistical analysis of the energy dispersive spectroscopy data is $Ba_2Co_{0.97}Ru_{1.03}O_6$ within error limits, affirming that our sample is homogeneous and single phase. Temperaturedependent synchrotron XRD (SXRD) measurements were performed at the Indian beamline (PF-18B) at Photon Factory, KEK, Japan using an x-ray wavelength of 0.8313 Å. Neutron powder diffraction (NPD) was performed at DMC (cold neutron diffractometer) at Paul Scherrer Institute using a neutron beam wavelength of 2.458 Å. Rietveld and Le-Bail refinements were performed using the FULLPROF SUITE [16] as well as JANA2020 [17] to analyze the diffraction data and obtain structural information. Crystal structures were generated using VESTA [18]. Specific heat and magnetic measurements were made using a Quantum Design physical property measurement system and MPMS-XL SQUID magnetometer, respectively. Resistivity and dielectric measurements were performed on a homemade setup. Dielectric spectroscopy was performed using a Novocontrol Alpha-A impedance analyzer in the frequency range of 1 Hz–1 MHz.

III. RESULTS AND DISCUSSION

All peaks of the SXRD and NPD patterns of Ba_2CoRuO_6 were indexed and refined with the 6H structure in space group $P6_3/mmc$ (Fig. 2), with lattice parameters $a = b =$ 5.700(4) Å and $c = 13.970(1)$ Å consistent with previous reports [15,19]. Structural parameters calculated at room temperature from synchrotron and neutron-diffraction data were found to be consistent confirming the quality of refinement (Fig. 1) and are tabulated in Table I. Oxygen positions were refined only using neutron data and no significant variation in oxygen occupancies was observed. We find that Co^{3+} fully occupies the corner sites and forms layers of triangular lattices perpendicular to the c axis [Fig. 2(b)] while there is significant antisite disorder in the dimer $4f(\frac{1}{3}, \frac{2}{3}, z)$ sites with Co^{3+} occupying about 30% of them. These sites form their own triangular layer in the a-b plane and the two corner-sharing octahedra also form a buckled honeycomb lattice.

Table II lists all the bond lengths and angles calculated from the refined structure and Fig. 2(c) visualizes them. The average distance between the dimer cations obtained from the refinement is 2.638 Å, which is smaller than that of the Ru-Ru metallic bond length (2.6725 Å [20]), implying that the intradimer antiferromagnetic (AFM) direct exchange has significant strength. The average (Ru/Co2)-O distance is ~1.97 Å, which matches almost perfectly with the expected value for a Ru^{5+}-O^{2-} bond [21], thus confirming that the material has a Co^{3+}/Ru^{5+} distribution instead of Co^{4+}/Ru^{4+} or Co^{2+}/Ru^{6+}. The Ru^{5+} ions are also slightly displaced from their centers due to Coulomb repulsion as is evident from the difference in the [(Ru/Co2)-O1 ~ 2.0246 Å] and [(Ru/Co2)-O2 ~ 1.9141 Å] bond lengths.

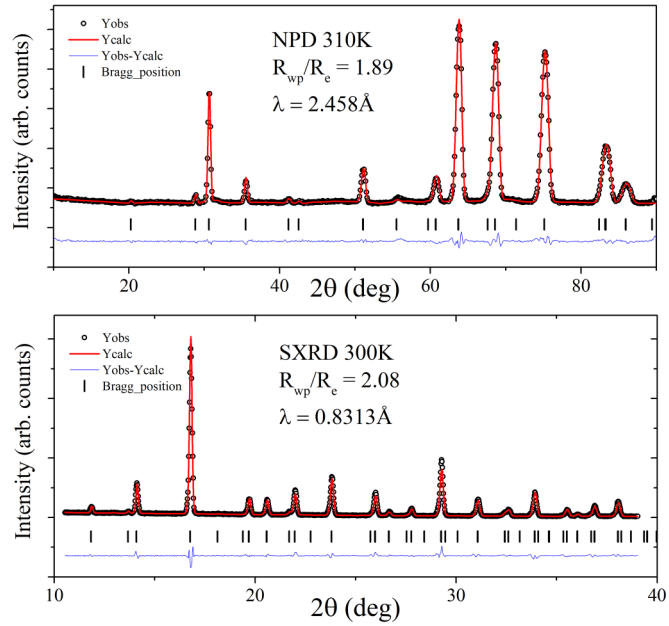

FIG. 1. Neutron powder diffraction (NPD; top) and synchrotron x-ray diffraction (SXRD; bottom) profiles at room temperature refined using the FULLPROF suite.

The spin-state flexibility of Co^{3+} opens up the possible existence of low-spin (LS), high-spin (HS), or intermediate spin (IS). The factors affecting the spin state of Co here are the oxidation state, the surrounding crystal field, the coordination number and the local symmetry, and the type of neighboring ions. A LS Co^{3+} is well documented and has been found in $LiCoO_2$ [22] and $La_2Li_{0.5}Co_{0.5}O_4$ [23]. HS Co^{3+} has been documented in weaker crystal fields such as in $YBaCo_4O_7$ with a tetrahedral local symmetry [24], and in Sr_2CoO_3Cl [25] and $BiCoO_3$ [26] with a square pyramidal local symmetry. The HS Co^{3+} in octahedral coordination is much rarer and has been seen only in systems with a LS-HS mix ($LaCoO_3$ [27], $Pr_{0.5}Ca_{0.5}CoO_3$ [28]) or with oxygen deficiency ($RBaCo_2O_{5.5}$ (R = rare-earth metal) [29,30], $Sr_{1-x}Y_xCoO_{3-\delta}$) [31]. There is also a continuing debate on whether the observed spin state is actually a mixture of HS and LS, or is a pure IS state.

TABLE I. Structural parameters of Ba_2CoRuO_6 obtained from Rietveld refinement of the neutron-diffraction pattern measured at 310 K. Space group: $P6_3/mmc$ (hexagonal). $a = b = 5.700(4)$ Å, $c = 13.970(1)$ Å, $\alpha = \beta = 90°$, $\gamma = 120°$.

Atom	Wyckoff	x	y	z	B	Occ.
Ba1	2b	0	0	1/4	0.0005	1
Ba2	4f	1/3	2/3	0.90963	0.0005	1
Co1	2a	0	0	0	0.24289	1
Co2	4f	1/3	2/3	0.15561	0.21454	0.30
Ru2	4f	1/3	2/3	0.15561	0.21454	0.70
O1	6h	0.48892	−0.02223	0.25	0.25418	0.97
O2	12k	0.16892	0.33811	0.41713	0.52233	1

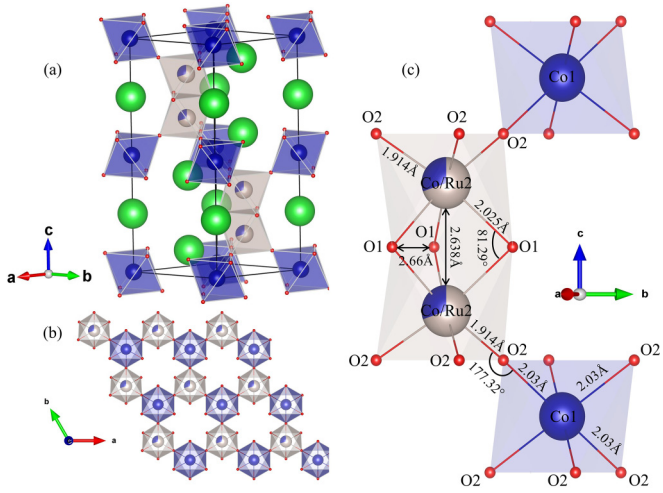

FIG. 2. (a) Hexagonal structure of Ba_2CoRuO_6 showing corner and face-shared octahedra. (b) Buckled honeycomb lattice formed by the corner sharing of B and B' ions. (c) Bond lengths and bond angles in the $(Co/Ru)_2O_9$ dimers and CoO_6 octahedra.

A pressure dependent study of the spin state of the octahedrally coordinated Co^{3+} in the $3d/4d$ transition metal oxide $SrCo_{0.5}Ru_{0.5}O_{2.96}$ [32] concludes that at room temperature and ambient pressure, the Co ions are in a HS state. Applying pressure induces a complete HS → LS transformation with no intermediate IS state. The crossover lies at about 1.93 Å Co-O bond length where the HS and LS states are strongly mixed and local lattice relaxations are allowed. Calculations using the configuration interaction cluster model indicate that the extremely large distortions are needed to stabilize an IS state. Another study on the evolution of the spin state of Co^{3+} in CoO_6 octahedral environment in $Sr_2Co_{0.5}Ir_{0.5}O_4$ [33] also finds that for an IS state to be stabilized there should be a strong elongated tetragonal distortion along with a short in-plane Co-O bond length. For in-plane Co-O bonds larger than 1.9 Å the IS state is highly unfavorable. A stable HS state is seen at high temperatures and ambient pressures (Co-O in plane = 1.944 Å, Co-O apex = 2.025 Å) which transforms completely into an LS state (Co-O in plane = 1.815 Å, Co-O apex = 1.925 Å) beyond 9.7 GPa again without encountering the IS state at all. In $LaCoO_3$, the Co-O bond length decreases from 1.9329 to 1.888 Å with increasing pressure, crossing a mixed HS-LS state to a pure LS state. The mixed spin state is due to shorter bond lengths (Co-O in plane = 1.967 Å, Co-O apex = 2.02 Å), close to the boundary of HS and LS. Clearly, the correlation between the spin state of Co and its distance from O is an effective indirect way to gauge the spin state of Co^{3+} ions.

TABLE II. Bond angles and lengths for Ba_2CoRuO_6 obtained from Rietveld refinement of neutron-diffraction data collected at 310 K.

Ba1-O1	×6	2.8527(3) Å
Ba1-O2	×6	2.8703(2) Å
Ba2-O1	×3	2.838(3) Å
Ba2-O2	×6	2.8525(3) Å
Ba2-O2′	×3	2.914(3) Å
Co1-O2	×6	2.0315(1) Å
(Ru/Co2)-O1	×3	2.0246(2) Å
(Ru/Co2)-O2	×3	1.9141(2) Å
(Ru/Co2)-O (avg)		1.9693(2) Å
Co1-(Ru/Co2)		3.9445(2) Å
(Ru/Co2)-(Ru/Co2)		2.638(6) Å
O1-(Ru/Co2)-O1		82.13(9)°
O1-(Ru/Co2)-O2		91.39(1)°
O2-(Ru/Co2)-O1		171.41(1)°
O2-Co1-O2		90.74(4)°
Co1-O2–(Ru/Co2)		177.32(8)°
(Ru/Co2)-O1–(Ru/Co2)		81.29(1)°

In this context, Ba_2CoRuO_6 is most likely to stabilize a HS state since there is no distortion in either of the two distinct octahedra encountered here with fairly large average bond lengths. The corner-shared CoO_6 octahedra contain equidistant in- and out-of-plane Co-O bonds (2.0315 Å). The octahedra that are shared also have equal in- and out-of-plane average bond lengths (1.9694 Å). These values are close to the HS state bond distances in $Sr_2Co_{0.5}Ir_{0.5}O_4$ and $SrCo_{0.5}Ru_{0.5}O_{2.96}$, implying that here too, the crystal field is fairly weak and is likely to favor an HS state at high temperatures. The stoichiometry calculated from the neutron-diffraction analysis is $Ba_2Co_{1.03}Ru_{0.97}O_{6-\delta}$ with $\delta = 0.07$, which points to a slight oxygen deficiency similar to $SrCo_{0.5}Ru_{0.5}O_{2.96}$ and validating our claim of an expected HS state for Co^{3+} in this compound. Cooling the sample causes only marginal changes in the bond lengths, indicating no significant change in Co^{3+} spin states on cooling, and the octahedra remain regular with the average in-plane and apex bond lengths Co1 octahedra = 2.0226 Å and Co/Ru2 octahedra = 1.9617 Å. Thus, we can conclude that the Co ions remain in a HS state between 2 and 300 K in this system.

The Co/Ru2-O–Co/Ru2 superexchange ($\angle_{ROR} = 81.29°$) competes with the intradimer direct exchange by favoring a weak ferromagnetic (FM) coupling. Direct exchange between Co^{3+} ions is not expected since the $3d$ orbitals are not extended enough. For the interactions between (Ru^{5+}:t_{2g}^3) and (Co^{3+}:$t_{2g}^4 e_g^2$), depending on which orbital of Co participates in exchange (t_{2g}/e_g), the interaction may be FM/AFM, respectively. There will also be a finite contribution from next-nearest neighbor exchange. All of these competing interactions are randomly distributed throughout the lattice due to the antisite disorder, implying that exchange randomness is a key player in dictating the physics of this system. The O1-O1 distance is small (∼2.661 Å) and allows the shared face of the octahedra to effectively shield the cationic repulsion [34], similar to other 6H perovskites [35,36].

dc magnetic susceptibility (χ_{dc}) of the sample measured at 5 KOe (Fig. 3), shows a cusp in the zero-field cooled (ZFC) curve accompanied by a bifurcation between the ZFC and field cooled (FC) curves around $T_f = 43$ K reminiscent of a spin-glass (SG) like behavior [37]. Canonical spin glasses generally show a temperatureindependent FC magnetization (M_{FC}) below T_f and this feature is often used to distinguish them from a superparamagnet (SPM) [38]. However, it is also possible for SPMs with a narrow volume distribution to show this plateau below the blocking temperature [39]. On the contrary, our FC curve continues to increase below

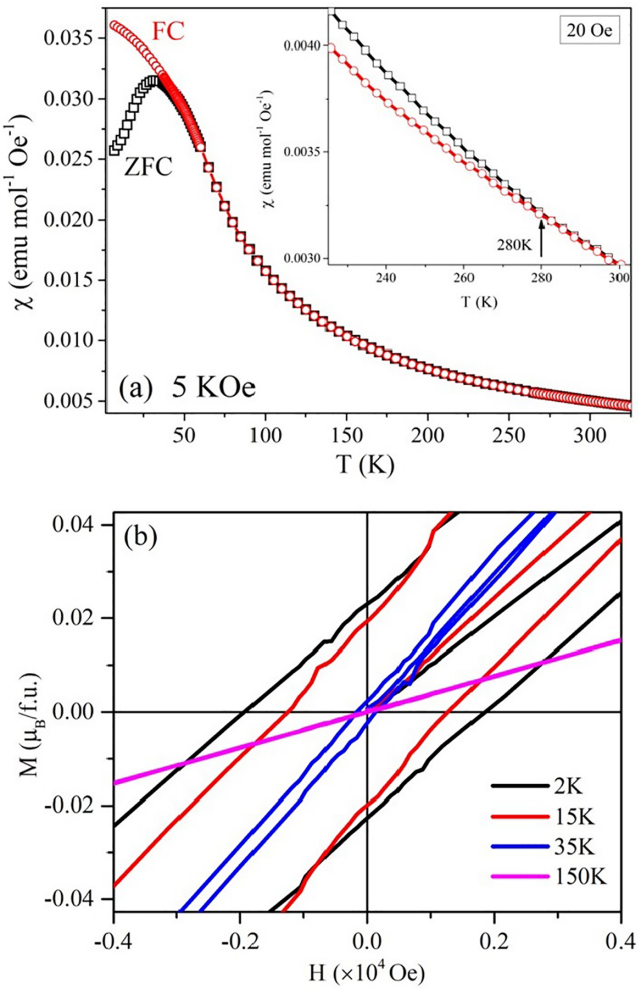

FIG. 3. (a) Temperature dependent dc susceptibility (χ_{dc}) measured at 5 KOe showing bifurcation between ZFC and FC curves below 47 K. Inset: χ_{dc} measured at $H = 20$ Oe showing the separation of ZFC and FC curves at 280 K. (b) $M(H)$ curves showing small, but finite hysteresis below T_f indicating a weak FM contribution.

T_f, a behavior also documented in various cluster glasses (CGs) [40–42]. Attempts to fit $\chi_{dc}^{-1}(T)$ to the Curie-Weiss (CW) law at high temperature failed (not shown here), as we encountered varying values of the Weiss temperature (θ_{CW}) and Curie constant (C) on changing the fitting (temperature) range, indicative of a rounding of χ^{-1}. This deviation from the CW linearity could be suggestive of clustering [38], implying that the system is not fully paramagnetic at room temperature. χ_{dc} at low fields ($H = 20$ Oe) shows that irreversibility occurs at temperatures as high at 280 K [inset of Fig. 3(a)]. In both SGs and SPMs, the existence of a finite dipolar interaction can cause the ZFC and FC curves to split at temperatures much higher than T_F (or T_B) and continue to rise as the sample is cooled [39,43]. This separation of ZFC and FC curves above the ZFC maxima with growing M_{FC} below the bifurcation point has also been observed in many other cluster glasses [39–41,44–46]. The temperature variation of lattice parameters [inset (a) of Fig. 4] obtained from Le Bail fits of synchrotron patterns measured at different temperatures also shows sharp changes at 50 and 280 K, consistent with the

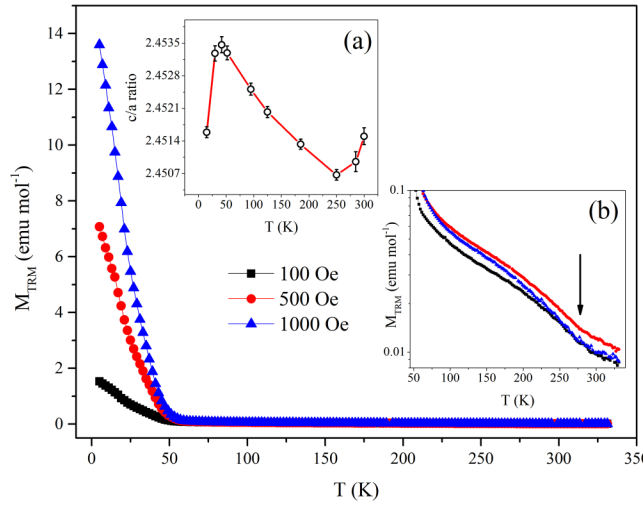

FIG. 4. Thermoremanent magnetization (M_{TRM}) vs temperature (T) measured in zero field in warming mode (using three different cooling fields). (a) Thermal variation in lattice parameters extracted from SXRD data showing features at 47 and 250 K. (b) Semilogarithmic plot of M_{TRM} vs T highlighting the subtle change of slope at 280 K (indicated using the arrow).

magnetization data, the former reflecting the freezing transition and the latter associated with the onset of magnetic correlations. We pick up a signature of these short-range correlations at ∼280 K in the thermoremanent magnetization (TRM) measurements (Fig. 4) as well, which have been useful in studying glassy behavior [47–49]. In this experiment, the sample is cooled to $T < T_f$ in the presence of an external field and then the field is turned off. $M_{TRM}(T)$ is then measured keeping $H = 0$ in warming mode. TRM being a zero-field measurement allows us to observe the thermal evolution of the magnetic state while being more sensitive to the antiferromagnetic order within clusters which would otherwise be suppressed by the paramagnetic contribution. Along with the huge upturn at T_f, we clearly capture a small change of slope around 280 K [inset (b) of Fig. 4] confirming that nucleation of spin clusters begins close to room temperature. The field dependence of M_{TRM} in this region is unlike that below T_f due to the fact that being a zero-field measurement, at such low moment values, the effect of the remnant field of the superconducting magnet of the magnetic property measurement system (MPMS) superconducting quantum interference device (SQUID) becomes relevant. Careful high-temperature magnetic susceptibility measurements would be essential to access the true paramagnetic region for this system.

To confirm if the ZFC-FC bifurcation in the dc susceptibility indeed corresponds to a cooperative freezing of spins, we measure the frequency dependence of the ac magnetic susceptibility (χ_{ac}) with temperature. Figure 5(a) shows the real part of χ_{ac} measured with an excitation field of $H = 2.6$ Oe after cooling the sample in zero field. The temperature of the ZFC magnetization (M_{ZFC}) peak shows a small shift with frequency attesting to the glassiness of this transition. This shift is quantified in the Mydosh parameter (δT_f),

$$\delta T_f = \frac{\Delta T_f}{T_f \Delta(\log_{10}\omega)}, \tag{1}$$

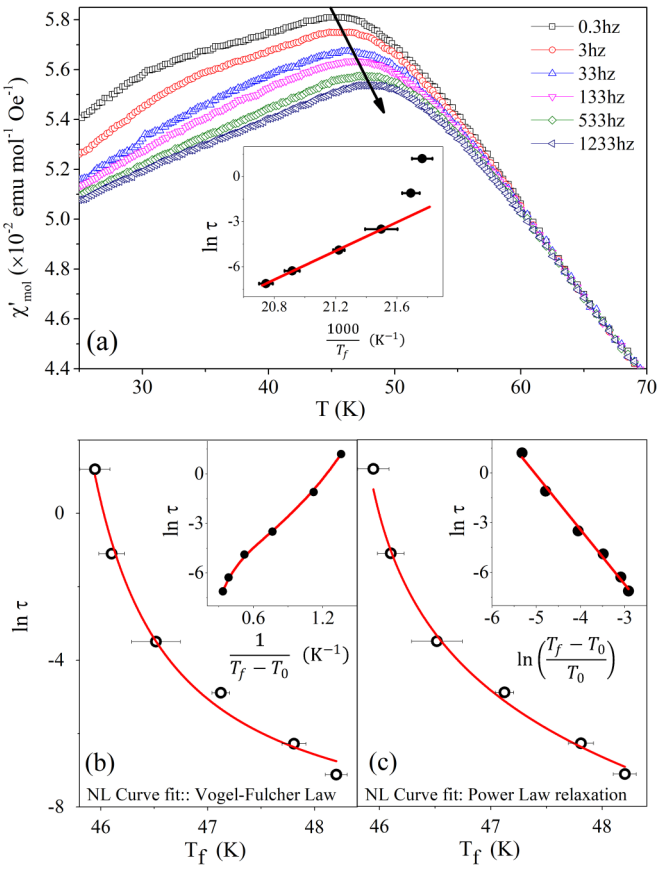

FIG. 5. (a) Real part of χ_{ac} as a function of temperature for different frequencies. Inset: $\ln\tau$ plotted against $1000/T_f$ showing nonlinear (non-Arrhenius) behavior. (b) $\ln\tau$ vs T_f nonlinear curve fit to the Vogel-Fulcher law. Inset: $\ln\tau$ $1/(T_f - T_0)$ using T_0 obtained from nonlinear fit showing nonlinearity. (c) Power-law fit to $\ln\tau$ vs T_f, Inset: the linear scaling of power-law fit.

which in our case is 0.0136. Here, T_f is the temperature at which the cusp occurs in $\mathrm{Re}(\chi_{ac})$ at a certain angular frequency ($\omega = 2\pi f$, f being the applied frequency in hertz). This value is higher than typical canonical spin glasses like CuMn (0.005) but matches well with values observed for reentrant spin glasses [50] and cluster glasses [46,51–53]. This distinguishes it from a SPM where this frequency shift is expected to be larger and δT_f is > 0.1 [50]. The logarithmic relaxation time $\ln\tau$ ($\tau = \frac{1}{\omega}$) also deviates strongly from linearity when plotted against $1000/T_f$ [inset of Fig. 5(a)] ruling out the possibility of a SPM-like thermally activated blocking (Arrhenius-like behavior) of spin clusters. Fitting $\ln\tau$ vs T_f to the Vogel-Fulcher (VF) law,

$$\tau = \tau_0 \exp\left(\frac{E_a}{k_B(T - T_0)}\right) \tag{2}$$

gives a better fit [Fig. 5(b)] resulting in parameters $\tau_0 \approx 10^{-4}$ s, $T_0 = 45.21 \pm 0.11$ K, and $E_a = 0.65 \pm 0.18$ meV. The VF law is an empirical law which is generally used to describe the viscosity of supercooled liquids and real glasses. It is essentially a modified version of the Arrhenius law, with T_0 as an extra parameter. A concrete physical interpretation of T_0, however, remains elusive [50]. A linear scaling of the

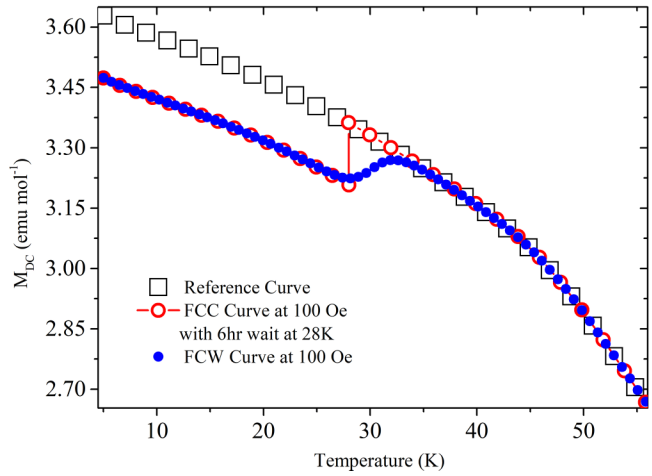

FIG. 6. Observation of the memory effect in Ba_2CoRuO_6 at $T = 28$ K ($< T_f$) with a waiting time of 6 h, using a cooling field of 100 Oe.

nonlinear fit to Eq. (2) reveals the fit to be unsatisfactory [inset of Fig. 5(b)] and hence, we look to the standard theory of phase transitions where dynamical scaling near the transition expects τ to vary as

$$\tau = \tau_0 \left(\frac{T_f}{T_0} - 1\right)^{-z\nu}, \tag{3}$$

where τ_0 is the characteristic relaxation time, T_0 the transition temperature, and $z\nu$ the dynamical exponent that encapsulates the critical slowing down of relaxation dynamics near the phase transition. A nonlinear fit to Eq. (3) and its linear scaling is shown in Fig. 5(c) and its inset, respectively. It is evident that the linear fit is drastically improved for Eq. (3). The parameters obtained from the fit are $T_0 = 45.72 \pm 0.03$ K, $\tau_0 = 6.22(\pm 0.19) \times 10^{-8}$ s, and $z\nu = 3.29 \pm 0.12$. When compared to typical values for a canonical spin glass CuMn (4.6 at. %; $\tau_0 = 10^{-12}$ s and $z\nu = 5.5$) we can see that the relaxation times of the two systems differ by almost four orders of magnitude demonstrating that the entities that respond to the external perturbation in this system are not individual spins but correlated, interacting spin clusters. The value of $z\nu$ is also lower than its typically observed range for SGs (4–12) [50]. However, $z\nu < 4$ has also been reported in some CG systems [53–55]. A low value of $z\nu$ approaching that for a mean-field phase transition ($z\nu = 2$) has been recognized as a marker of strong interactions allowing cooperative freezing of magnetic moments at T_f [56].

Ba_2CoRuO_6 also shows the classic glassy behavior of retaining the *memory* of an aging process within the frozen state. For this experiment, a reference FC curve is first measured by normally cooling the sample in $H = 100$ Oe and then measuring M_{FC} during warming. The sample is then cooled again in field from $T > T_f$ but this time, on reaching $T = 28$ K $< T_f$, the field is switched off and the magnetization is allowed to relax. After $t_w = 6$ h, the field is switched back on and the sample is allowed to continue cooling normally to the lowest temperature and magnetization is measured during warming. As evident from the inset of Fig. 6, the material *remembers* the aging it underwent during cooling and smoothly merges

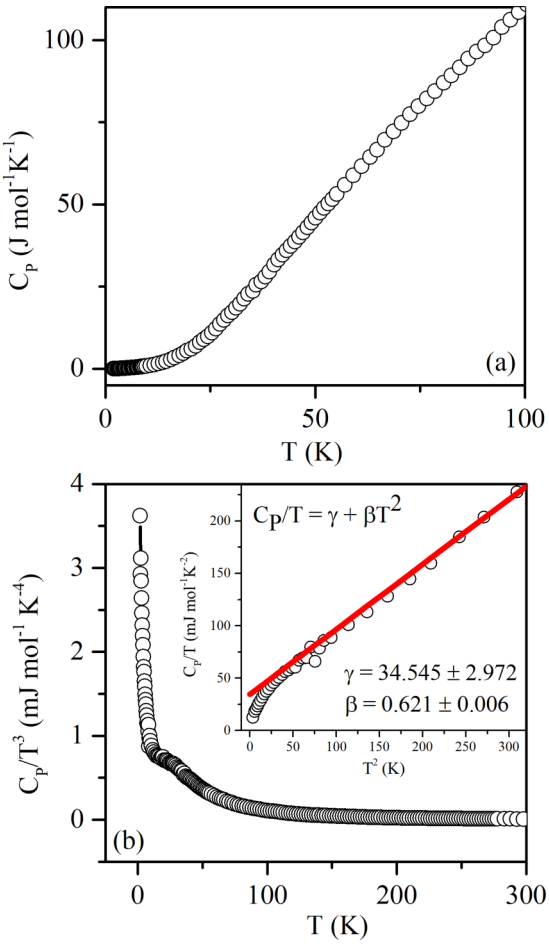

FIG. 7. Plots of (a) C_P vs T showing the absence of any feature in the vicinity of T_f, and (b) C_P/T^3 plotted against T showing a sharp upturn below T_f. Inset of (b) shows C_P/T plotted against T^2 with its linear fit showing the deviation from the Debye behavior at low temperatures. The fitting equation as well the obtained fit parameters are also mentioned.

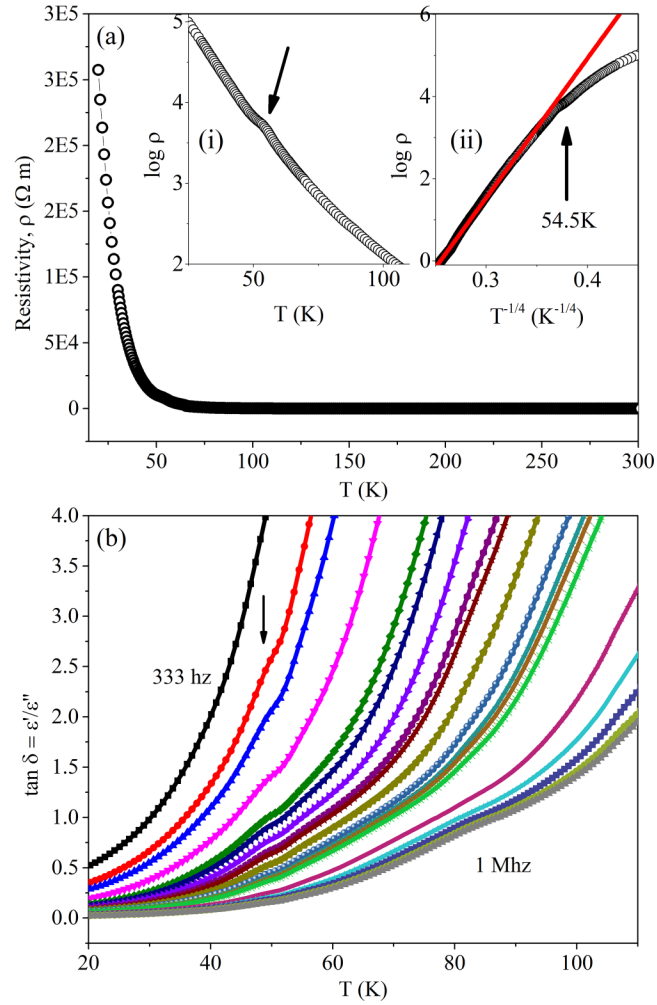

FIG. 8. (a) Temperature dependence of resistivity [$\rho(T)$] showing insulating behavior at low temperatures. Inset: (i) $\log_{10}\rho$ plotted against T shows a very small feature (indicated by the arrow) near T_f. (ii) $\log_{10}\rho$ plotted against $T^{-1/4}$ showing deviation from linearity below 55 K, implying that the 3D VRH model describes the conductivity well until the glass transition is approached. (b) Dielectric loss tangent ($\tan\delta = \epsilon''/\epsilon'$) plotted as a function of temperature also shows a subtle feature close to 50 K hinting at a weak magnetodielectric coupling.

into the previously measured cooling curve revealing (and simultaneously, erasing) the memory [57]. This clear evidence of magnetic memory in the system reaffirms the glassiness of the low-temperature state of Ba_2CoRuO_6.

Further confirmation that the magnetic transition at 43 K relates to a global freezing of spin clusters and not long-range ordering, comes from the specific heat of Ba_2CoRuO_6 measured in zero field, which is featureless around 50 K [Fig. 7(a)] implying that the entropy change associated with this transition is negligible. A linear fit to C_P/T vs T^2 in the low-temperature regime shown in the inset of Fig. 7(b) gives $\gamma = 34.55 \pm 2.97$ mJ mol^{-1} K^{-2} and $\beta = 0.62 \pm 0.01$ mJ mol^{-1} K^{-4}. The γ value is unusually large for an insulating system but this, along with the downturn below ~10 K can also be attributed to the glassy ground state. High values of γ have also been reported in various other frustrated systems including 6H triple perovskites [49,58,59] and half-doped manganites [60,61]. These parameters allow us to calculate the Debye temperature (θ_D) using the relation

$$\theta_D = \left(\frac{12\pi^4 pR}{5\beta}\right)^{1/3}, \tag{4}$$

where p is the number of atoms per formula unit (=10 for double perovskites) and R is the gas constant. We obtain a value of $\theta_D = 315.14$ K $\pm$ 1.01 K, which is close to the typically observed values for perovskites (350–400 K) [61,62]. C_P/T^3 plotted against T [Fig. 7(b)] shows an upturn below 10 K which is related to a presence of tunneling in two-level systems and is often seen in glassy/phase-separated systems [49,60,63]. In Debye materials, where periodicity is expected, C_P/T^3 is just expected to flatten out at low temperature.

Resistivity measurements show semiconducting behavior between 20 and 300 K with a small feature in the vicinity of T_f. Linearity up to temperatures approaching T_f is obtained when $\ln\rho$ is plotted against $T^{-1/4}$ [inset (ii) of Fig. 8(a)], suggesting that it is the three-dimensional (3D) Mott variable

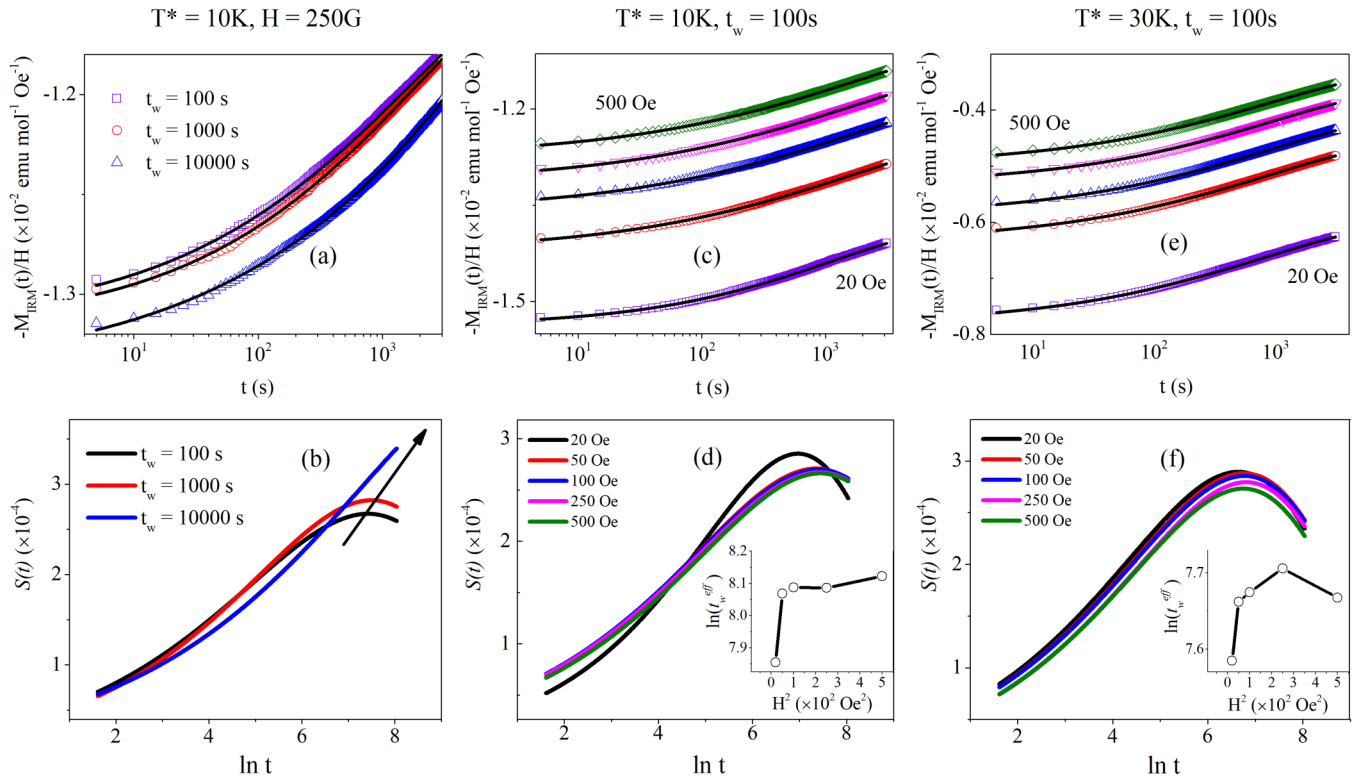

FIG. 9. Time dependence of isothermal remnant magnetization ($M_{\rm IRM}$) plotted in the form of $-M_{\rm IRM}(t)/H$ vs time t for (a) different waiting times at 10 K, and different fields at (c) 10 K and (e) 30 K. Solid lines denote analytical fit using a modified stretched exponential. (b), (d), and (f) show $S(t)$ vs t calculated from the fits shown in (a), (c), and (e), respectively. Insets of (d) and (f) show a plot of $\ln(t_w^{\rm eff})$ vs H^2 showing the lack of variation in $t_w^{\rm eff}$ with applied magnetic field.

range hopping (VRH) model,

$$\rho = \rho_0 \exp\left[\left(\frac{T_0}{T}\right)^{1/4}\right], \tag{5}$$

that likely governs the conduction mechanism in this temperature range. This mechanism is known to describe the low-temperature conduction in disordered systems with localized charge-carrier states, and conduction in other 6H perovskites is also reported to behave similarly [10,64,65]. The three-dimensional conduction suggests that the interlayer and intralayer hopping integrals are of similar energies and all exchange pathways participate in conduction. Below T_f, the material becomes highly insulating due to increased localization/freezing of these hopping electrons. Dielectric spectroscopy with an excitation field of $V_{\rm ac} = 1$ V in the frequency range 0.3 KHz–1 MHz reveals Ba_2CoRuO_6 to be an extremely lossy dielectric for $T > 150$ K. Below 150 K, ϵ' and ϵ'' decrease smoothly and do not show any marked features; however, on close inspection, a very subtle frequency dependent feature can be seen near 50 K in the loss tangent ($\tan\delta = \epsilon''/\epsilon'$) [Fig. 8(b)]. This could point to the existence of a weak magnetodielectric coupling;however, extensive magnetic field dependent dielectric measurements would be required to confirm this.

To further probe the nonequilibrium relaxation dynamics of the frozen state, we perform field (H) and waiting time (t_w) dependent aging experiments using the following protocol: the sample is cooled in the presence of a finite field from $T > T_f$ to $T^* < T_f$ and after waiting for time t_w, the field is switched off and the magnetization is allowed to relax. We measure this relaxation with time for ∼2 h. This isothermal remnant magnetization ($M_{\rm IRM}$) follows the stretched exponential function

$$M_{\rm IRM}(t) = M_0 + A\exp\left[-\left(\frac{t}{\tau}\right)^{1-n}\right], \tag{6}$$

which is typically used to describe the slow dynamics of spin glasses. Here, M_0 is the static magnetization, A is the relaxing, glassy component, τ is the characteristic relaxation time, and n is the time-stretching exponent. The value of n critically governs the exact relaxation rate and is expected to lie around 0.5 for spin glasses. For all our fits for different t_w and H [Figs. 9(a), 9(c) and 9(e)], the value of n is always found to vary between 0.5 and 0.6, confirming that the relaxations are slower than exponential. At a given temperature, t_w is proportional to the size of the frozen domains. Waiting for a longer time allows one to probe the aging behavior of larger domain sizes [66] with longer relaxation times. As a result, when the waiting times are increased, so do the effective response times of the large clusters [67]. The response function $S(t)$ given b:

$$S(t) = \frac{d}{d\ln(t)}\left(\frac{-M_{\rm IRM}(t,t_w)}{H}\right) \tag{7}$$

is expected to peak at a time of the order of t_w. This is reflected in Fig. 9(b) where $S(t)$ peaks can be seen shifting towards longer timescales with increasing waiting times. The only exception is found for $t_w = 100$ s where $S(t)$ peaks around the same time as $t_w = 1000$ s albeit slightly earlier. This could be related to the time required for temperature and field stabilization during the measurement, which would affect the lower waiting times more, since these two timescales are of similar orders of magnitude.

We also probe the magnetic field dependence of aging to estimate the SG correlation length from the variation of the effective waiting time t_w^{eff} [the time at which $S(t)$ peaks] with H^2. $S(t)$ is linked to the overall height of the energy barriers available, which changes as a function of the external magnetic field. When the field is increased, these effective barrier heights are reduced and thus, smaller values of t_w^{eff} are expected as the field is increased [68,69]. Curiously, we see $S(t)$ peaking at (slightly) higher timescales with increasing H [Figs. 9(d) and 9(f)]. However, a closer look reveals that the change is minuscule (of only a few tens of seconds). This means $S(t)$ does not appreciably shift its peak from the vicinity of t_w between 20 and 500 Oe and the value of τ essentially remains unchanged ($\sim 10^3$ s) through different external fields. This is interesting since the magnetic (Zeeman) energy (E_z) associated with a change in field H, is related to the volume over which the spins are locked together for barrier hopping (N_s) as $E_z = N_s \chi_{\text{FC}} H^2$ where χ_{FC} is the field cooled susceptibility per spin. The spin glass correlation length ξ is the radius of this volume N_s. If N_s is built of smaller clusters, the activation energy corresponds to smaller barrier heights and $S(t)$ always peaks around the waiting time t_w (which is fixed), thus returning similar t_w^{eff} for different applied fields [68]. This is precisely what we find in our measurements and this validates our claim of a cluster glass ground state for this system. However, since no field dependence was found, we were unable to calculate the SG correlation length using this method.

Magnetization measured under various applied fields reveals that T_f is strongly suppressed at higher fields (Fig. 10). Fitting $T_f(H)$ (Fig. 10) to the mean-field relation for vector spin glasses with random anisotropy [70],

$$T_f(H) = T_f(0)(1 - AH^p), \tag{8}$$

gives $p \approx 0.45$ and $T_f(0) \approx 42.8$ K. $T_f(0)$ is the temperature where the ZFC curve is expected to peak in the absence of an external magnetic field. A is a constant parametrizing the randomly distributed exchange term and p is an exponent that depends on the strength of anisotropy with respect to the magnetic field. When anisotropy is strong, $p = \frac{2}{3} \approx 0.67$, corresponding to the A-T (de Almeida and Thouless) line for Ising spins [71], is expected. TheGabay and Toulouse line [72] with $p \approx 2$ is expected in Heisenberg spin systems with weak anisotropy where two transitions are predicted to mark the distinct freezing of transverse and longitudinal spins. Our value of $p \sim 0.45$ is closer to the A-T value suggesting that we are in the strong anisotropy regime. This anisotropy is most likely a result of the globally disordered distribution of the various exchange interactions present in this system, forming short-range ordered regions of varying sizes, which continue to compete with each other down to the lowest temperatures, neither being able to establish a long-range ordered ground state.

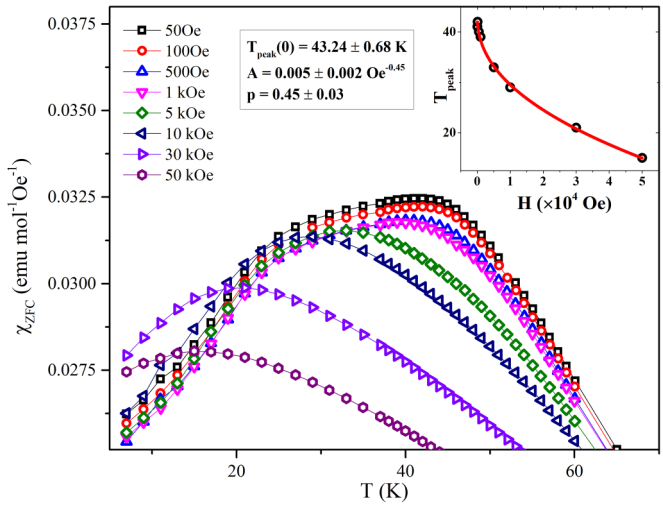

FIG. 10. Suppression of the ZFC maxima with increasing magnetic field $H = 50$ Oe to 50 kOe. Inset: Temperature corresponding to the ZFC peak (T_{peak}) plotted against applied field H and fitted to the equation $T_f(H) = T_f(0)(1 - AH^p)$; parameters obtained from the fit are displayed alongside.

NPD patterns were also measured at temperatures 150, 20, and 1.7 K to probe the magnetic structure within the frozen spin clusters below T_f. Below 20 K, two extremely weak reflections are observed at $2\theta = 17.5^\circ$ and 39.5°. A comparison between the diffraction profile at 310 and 1.7 K is shown in Fig. 11 illustrating the magnetic Bragg reflections. Using the K-SEARCH program in the FULLPROF suite [16], we find that the k vector that generates these magnetic peaks is $(\frac{1}{2},0,0)$ [equivalent to $(0,\frac{1}{2},0)$ and $(\frac{1}{2},\frac{1}{2},0)$] suggesting that an antiferromagnetic order with a magnetic unit cell doubling exists within the clusters. No significant enhancement of the crystallographically allowed peaks is observed, ruling out ferromagnetic order. However, we do observe hysteresis loops in $M(H)$ measurements which widen on cooling the sample (Fig. 3). Although the coercivity at 2 K is 1.9 kOe, no saturation is observed. This reveals the persistence of a small weak FM contribution that continues to compete with the dominant AFM interactions in the CG phase.

Magnetic representation analysis was performed using SARAH [73,74] which resulted in only the odd irreps surviving for the corner sites (six basis vectors were projected), while all the irreps survived for the dimer sites (12 basis vectors were projected). On testing with various combinations of these irreps for both the sites, we eventually could see that Γ_1 and Γ_3 were identical to each other and both Γ_1 and Γ_7 gave good fits to both the magnetic peaks. This is shown in Fig. 11. For the sake of clarity we also show the fit using Γ_5 in Fig. 11 and it can be seen that it does not generate any intensity for the peak at 39.5°. So, we can conclude that the fits from Γ_1 and Γ_7 are of similar quality. Figure 12 shows the structures generated from each of these irreps. Both the structures show canted spins arranged antiferromagnetically along the c axis and ferromagnetically along b. The major difference between the two seems to be the direction of cant-

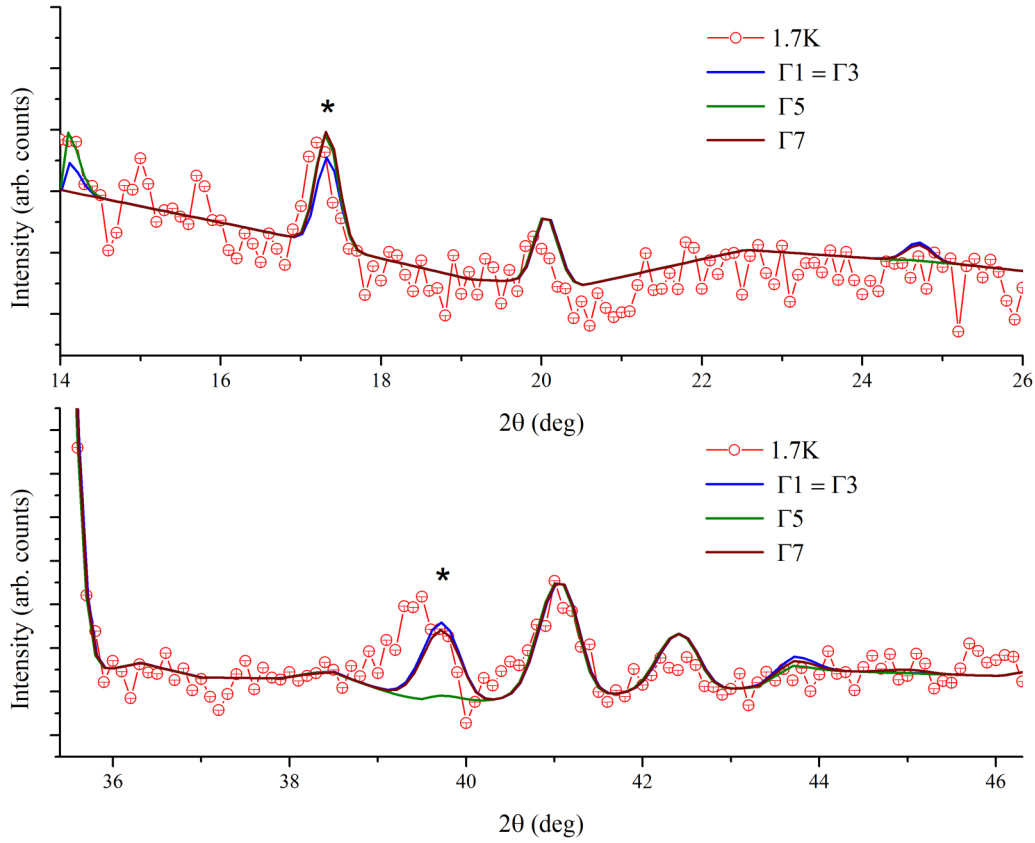

FIG. 11. Neutron powder diffraction profile measured at 1.7 K, showing additional peaks prohibited by the crystallographic space group $P6_3/mmc$ at $2\theta = 17.5^\circ$ and 39.5° marked with a * and their fits to three different irreps Γ1, Γ5, and Γ7.

ing. The Γ_1 structure has spins canted about the *a*-*b* plane, while in the Γ_3 structure they cant about the *c* axis. Since the moment values obtained from both these fits are similar, we cannot unambiguously identify the correct structure, and both of these are plausible. The moments within the dimers are antiferromagnetically coupled for both the structures so it makes sense that we get extremely small moments from those sites. Moment suppression is also observed on the sites solely occupied by Co and is likely the result of the strong disorder and exchange randomness immanent within this material [75].

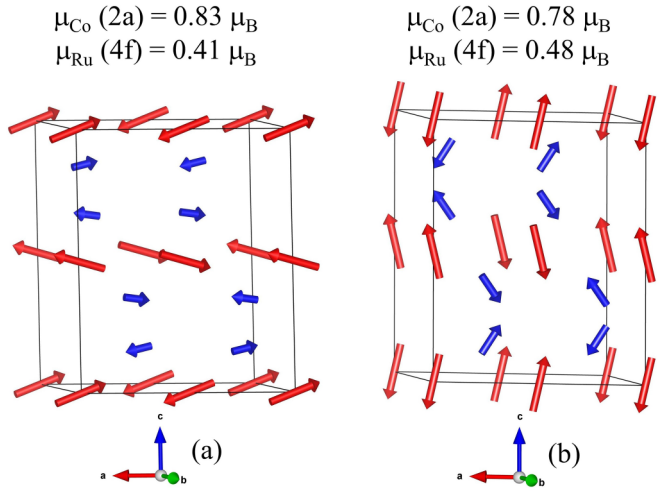

FIG. 12. The two plausible spin configurations within the frozen clusters obtained from magnetic structure refinement using the irreps (a) Γ_1 and (b) Γ_7 which gave the best fits to the neutron-diffraction data collected at 1.7 K. Both configurations result in similar goodness of fits and moment values on the two magnetic sites.

IV. CONCLUSIONS

We report an extensive study of the 6H disordered double perovskite Ba_2CoRuO_6 via synchrotron and neutron powder diffraction, ac and dc magnetization, waiting time and field dependent aging, resistivity, specific heat, and dielectric measurements and conclude it to be a disorder-driven cluster glass with a strong exchange anisotropy. The system shows classic glassy phase characteristics such as a frequency dependence in ac magnetization, a field dependent ZFC-FC bifurcation in dc magnetization, no saturation at high fields, robust memory and aging effects, as well as non-Debye behavior in the low-temperature specific heat, which is otherwise featureless. Through rigorous analysis of the ac susceptibility data we establish that the participating entities here are magnetic spin clusters that start forming near room temperature and continue to grow on further cooling. At the lowest temperature of 2 K, this system displays signatures of small AFM order (additional low angle peaks in neutron-diffraction pattern) within the frozen clusters, along with a weak FM contribution. Within the frozen clusters, the AFM order has a doubled

magnetic unit cell which is consistent with an arrangement of canted spins either about the *a*-*b* plane or the *c* axis with both AFM (along the *a* and *c* axis) and FM (along the *b* axis) correlations persisting and small moment values $< 1\mu_B$. This suggests that the system harbors a fierce competition between FM and AFM interactions which is strong enough to prohibit long-range ordering down to 2 K. Analysis of the T_f-H phase gives a p value which is also consistent with a system containing strong random anisotropy, even though it does not mark the existence of the A-T line. This exchange anisotropy promoted by the large disorder establishes a very frustrated network of Co^{3+} and Ru^{5+} ions. On cooling, strengthened local correlations lead to clustering of these ions in random regions forming both ferro- and antiferromagnetic domains which grow in size and strength until they undergo a cooperative global freezing at $T_f \sim 43$ K and form a cluster glass ground state.

ACKNOWLEDGMENTS

S.C. and S.N. thank the Department of Science and Technology, India (SR/NM/Z-07/2015) for financial support and the Jawaharlal Nehru Centre for Advanced Scientific Research (JNCASR) for managing the project. S.C. and S.N. acknowledge support from an Air Force Research Laboratory grant (Grant No. FA2386-21-1-4051). S.C. is thankful to J. R. Carvajal and Sudhindra Rayaprol for extensive discussions on magnetic structure solving using neutron-diffraction data. S.C. and S.N. thank A. K. Nigam for specific heat measurements. S.C. is thankful to Jitender Thakur for performing synchrotron measurements at PFKEK (Japan). This work is partly based on experiments performed at the Swiss spallation neutron source SINQ, Paul Scherrer Institute, Villigen, Switzerland.

[1] S. Vasala and M. Karppinen, $A_2B'B''O_6$ perovskites: A review, Prog. Solid State Chem. **43**, 1 (2015).

[2] S. A. J. Kimber, M. S. Senn, S. Fratini, H. Wu, A. H. Hill, P. Manuel, J. P. Attfield, D. N. Argyriou, and P. F. Henry, Charge Order at the Frontier between the Molecular and Solid States in $Ba_3NaRu_2O_9$, Phys. Rev. Lett. **108**, 217205 (2012).

[3] L. Shlyk, S. Kryukov, V. Durairaj, S. Parkin, G. Cao, and L. De Long, Magnetic, and electronic properties of a $Ba_3InRu_2O_9$ single crystal, J. Magn. Magn. Mater. **319**, 64 (2007).

[4] L. T. Nguyen and R. J. Cava, Hexagonal perovskites as quantum materials, Chem. Rev. **121**, 2935 (2021).

[5] D. Ziat, A. A. Aczel, R. Sinclair, Q. Chen, H. D. Zhou, T. J. Williams, M. B. Stone, A. Verrier, and J. A. Quilliam, Frustrated spin-$\frac{1}{2}$ molecular magnetism in the mixed-valence antiferromagnets $Ba_3MRu_2O_9$ (M = In, Y, Lu), Phys. Rev. B **95**, 184424 (2017).

[6] Q. Chen, S. Fan, K. M. Taddei, M. B. Stone, A. I. Kolesnikov, J. Cheng, J. L. Musfeldt, H. Zhou, and A. A. Aczel, Large positive zero-field splitting in the cluster magnet $Ba_3CeRu_2O_9$, J. Am. Chem. Soc. **141**, 9928 (2019).

[7] Q. Chen, A. Verrier, D. Ziat, A. J. Clune, R. Rouane, X. Bazier-Matte, G. Wang, S. Calder, K. M. Taddei, C. R. dela Cruz, A. I. Kolesnikov, J. Ma, J.-G. Cheng, Z. Liu, J. A. Quilliam, J. L. Musfeldt, H. D. Zhou, and A. A. Aczel, Realization of the orbital-selective Mott state at the molecular level in $Ba_3LaRu_2O_9$, Phys. Rev. Mater. **4**, 064409 (2020).

[8] A. A. Aczel, P. J. Baker, D. E. Bugaris, J. Yeon, H.-C. zur Loye, T. Guidi, and D. T. Adroja, Exotic Magnetism on the Quasi-fcc Lattices of the d^3 Double Perovskites $La_2NaB'O_6$ (B' = Ru, Os), Phys. Rev. Lett. **112**, 117603 (2014) .

[9] W. Xia, Q. Zhou, H. Xu, L. Chen, and J. He, Sr_2FeRuO_6: Magnetic and transport properties of the double perovskite, Physica B: Condens. Matter **403**, 2189 (2008).

[10] R. Phatak, K. Krishnan, S. K. Sali, A. Das, and A. K. Nigam, Structure and magnetic properties of Sr_2CoRuO_6, J. Magn. Magn. Mater. **344**, 129 (2013).

[11] J. P. Carlo, J. P. Clancy, K. Fritsch, C. A. Marjerrison, G. E. Granroth, J. E. Greedan, H. A. Dabkowska, and B. D. Gaulin, Spin gap and the nature of the $4d^3$ magnetic ground state in the frustrated fcc antiferromagnet Ba_2YRuO_6, Phys. Rev. B **88**, 024418 (2013).

[12] K. Yoshii, N. Ikeda, and M. Mizumaki, Magnetic and dielectric properties of the ruthenium double perovskites La_2MRuO_6 (M = Mg, Co, Ni, and Zn), Phys. Status Solidi A **203**, 2812 (2006).

[13] I. Terasaki, T. Igarashi, T. Nagai, K. Tanabe, H. Taniguchi, T. Matsushita, N. Wada, A. Takata, T. Kida, M. Hagiwara, K. Kobayashi, H. Sagayama, R. Kumai, H. Nakao, and Y. Murakami, Absence of magnetic long range order in $Ba_3ZnRu_2O_9$: A spin-liquid candidate in the $S = 3/2$ dimer lattice, J. Phys. Soc. Jpn. **86**, 033702 (2017).

[14] M. DeMarco, H. A. Blackstead, J. D. Dow, M. K. Wu, D. Y. Chen, F. Z. Chien, M. Haka, S. Toorongian, and J. Fridmann, Magnetic phase transition in superconducting $Sr_2YRu_{0.95}Cu_{0.05}O_6$ observed by the ^{99}Ru Mössbauer effect, Phys. Rev. B **62**, 14301 (2000).

[15] S. Kim and P. Battle, Structural and electronic properties of mixed Co/Ru perovskites $AA'CoRuO_6$ (A, A' = Sr, Ba, La), J. Solid State Chem. **114**, 174 (1995).

[16] J. Rodriguez-Carvajal, FULLPROF: A Program for Rietveld Refinement and Pattern Matching Analysis, in *Satellite Meeting on Powder Diffraction of the XV Congress of the IUCr, Toulouse, France*, Vol. 127 (1990).

[17] V. Petříček, M. Dušek, and L. Palatinus, Crystallographic computing system JANA2006: General features, Z. Kristallogr. - Cryst. Mater. **229**, 345 (2014).

[18] K. Momma and F. Izumi, VESTA 3 for three-dimensional visualization of crystal, volumetric and morphology data, J. Appl. Crystallogr. **44**, 1272 (2011).

[19] U. Hira, J. W. G. Bos, A. Missyul, F. Fauth, N. Pryds, and F. Sher, $Ba_{2-x}Bi_xCoRuO_6 (0.0 \leqslant x \leqslant 0.6)$ hexagonal double-perovskite-type oxides as promising p-type thermoelectric materials, Inorg. Chem. **60**, 17824 (2021).

[20] A. Jain, S. P. Ong, G. Hautier, W. Chen, W. D. Richards, S. Dacek, S. Cholia, D. Gunter, D. Skinner, G. Ceder, and K. A. Persson, The Materials Project: A materials genome approach to accelerating materials innovation, APL Mater. **1**, 011002 (2013).

[21] O. C. Gagné and F. C. Hawthorne, Bond-length distributions for ions bonded to oxygen: Results for the transition metals and quantification of the factors underlying bond-length variation in inorganic solids, IUCrJ **7**, 581 (2020).

[22] M. Oku, X-ray photoelectron spectrum of low-spin Co (III) in $LiCoO_2$, J. Solid State Chem. **23**, 177 (1978).

[23] Z. Hu, C. Mazumdar, G. Kaindl, F. De Groot, S. Warda, and D. Reinen, Valence electron distribution in $La_2Li_{1/2}Cu_{1/2}O_4$, $Nd_2Li_{1/2}Ni_{1/2}O_4$, and $La_2Li_{1/2}Co_{1/2}O_4$, Chem. Phys. Lett. **297**, 321 (1998).

[24] N. Hollmann, Z. Hu, M. Valldor, A. Maignan, A. Tanaka, H. H. Hsieh, H.-J. Lin, C. T. Chen, and L. H. Tjeng, Electronic and magnetic properties of the kagome systems $YBaCo_4O_7$ and $YBaCo_3MO_7$ (M = Al, Fe), Phys. Rev. B **80**, 085111 (2009).

[25] Z. Hu, H. Wu, M. W. Haverkort, H. H. Hsieh, H.-J. Lin, T. Lorenz, J. Baier, A. Reichl, I. Bonn, C. Felser, A. Tanaka, C. T. Chen, and L. H. Tjeng, Different Look at the Spin State of Co^{3+} Ions in a CoO_5 Pyramidal Coordination, Phys. Rev. Lett. **92**, 207402 (2004).

[26] A. A. Belik, S. Iikubo, K. Kodama, N. Igawa, S.-i. Shamoto, S. Niitaka, M. Azuma, Y. Shimakawa, M. Takano, F. Izumi *et al.*, Neutron powder diffraction study on the crystal and magnetic structures of $BiCoO_3$, Chem. Mater. **18**, 798 (2006).

[27] M. W. Haverkort, Z. Hu, J. C. Cezar, T. Burnus, H. Hartmann, M. Reuther, C. Zobel, T. Lorenz, A. Tanaka, N. B. Brookes *et al.*, Spin State Transition in $LaCoO_3$ Studied Using Soft X-Ray Absorption Spectroscopy and Magnetic Circular Dichroism, Phys. Rev. Lett. **97**, 176405 (2006).

[28] S. Tsubouchi, T. Kyomen, M. Itoh, P. Ganguly, M. Oguni, Y. Shimojo, Y. Morii, and Y. Ishii, Simultaneous metal-insulator and spin-state transitions in $Pr_{0.5}Ca_{0.5}CoO_3$, Phys. Rev. B **66**, 052418 (2002).

[29] C. Martin, A. Maignan, D. Pelloquin, N. Nguyen, and B. Raveau, Magnetoresistance in the oxygen deficient $LnBaCo_2O_{5.4}$ (Ln = Eu, Gd) phases, Appl. Phys. Lett. **71**, 1421 (1997).

[30] Z. Hu, H. Wu, T. Koethe, S. Barilo, S. Shiryaev, G. Bychkov, C. Schüßler-Langeheine, T. Lorenz, A. Tanaka, H. Hsieh *et al.*, Spin-state order/disorder and metal–insulator transition in $GdBaCo_2O_{5.5}$: experimental determination of the underlying electronic structure, New J. Phys. **14**, 123025 (2012).

[31] W. Kobayashi, S. Ishiwata, I. Terasaki, M. Takano, I. Grigoraviciute, H. Yamauchi, and M. Karppinen, Room-temperature ferromagnetism in $Sr_{1-x}Y_xCoO_{3-\delta}$ ($0.2 \leqslant x \leqslant 0.25$), Phys. Rev. B **72**, 104408 (2005).

[32] J.-M. Chen, Y.-Y. Chin, M. Valldor, Z. Hu, J.-M. Lee, S.-C. Haw, N. Hiraoka, H. Ishii, C.-W. Pao, K.-D. Tsuei *et al.*, A complete high-to-low spin state transition of trivalent cobalt ion in octahedral symmetry in $SrCo_{0.5}Ru_{0.5}O_{3-\delta}$, J. Am. Chem. Soc. **136**, 1514 (2014).

[33] Y.-Y. Chin, H.-J. Lin, Z. Hu, C.-Y. Kuo, D. Mikhailova, J.-M. Lee, S.-C. Haw, S.-A. Chen, W. Schnelle, H. Ishii *et al.*, Relation between the Co-O bond lengths and the spin state of Co in layered cobaltates: A high-pressure study, Sci. Rep. **7**, 3656 (2017).

[34] A. Santoro, I. Natali Sora, and Q. Huang, Bond valence analysis of $BaRuO_3$, J. Solid State Chem. **151**, 245 (2000).

[35] P. Lightfoot and P. D. Battle, The crystal and magnetic structures of $Ba_3NiRu_2O_9$, $Ba_3CoRu_2O_9$, and $Ba_3ZnRu_2O_9$, J. Solid State Chem. **89**, 174 (1990).

[36] P. Kayser, S. Injac, B. Ranjbar, B. J. Kennedy, M. Avdeev, and K. Yamaura, Magnetic and structural studies of Sc containing ruthenate double perovskites A_2ScRuO_6 (A = Ba, Sr), Inorg. Chem. **56**, 9009 (2017).

[37] K. Binder and A. P. Young, Spin glasses: Experimental facts, theoretical concepts, and open questions, Rev. Mod. Phys. **58**, 801 (1986).

[38] M. Giot, A. Pautrat, G. André, D. Saurel, M. Hervieu, and J. Rodriguez-Carvajal, Magnetic states and spin-glass properties in $Bi_{0.67}Ca_{0.33}MnO_3$: Macroscopic ac measurements and neutron scattering, Phys. Rev. B **77**, 134445 (2008).

[39] S. Nair and A. K. Nigam, Critical exponents and the correlation length in the manganite spin glass $Eu_{0.5}Ba_{0.5}MnO_3$, Phys. Rev. B **75**, 214415 (2007).

[40] D. A. Pejaković, J. L. Manson, J. S. Miller, and A. J. Epstein, Photoinduced Magnetism, Dynamics, and Cluster Glass Behavior of a Molecule-Based Magnet, Phys. Rev. Lett. **85**, 1994 (2000).

[41] M. Koyano, M. Suezawa, H. Watanabe, and M. Inoue, Low-field magnetization and AC magnetic susceptibility of spin- and cluster-glasses of itinerant magnet Fe_xTiS_2, J. Phys. Soc. Jpn. **63**, 1114 (1994).

[42] S. Mukherjee, R. Ranganathan, P. S. Anilkumar, and P. A. Joy, Static and dynamic response of cluster glass in $La_{0.5}Sr_{0.5}CoO_3$, Phys. Rev. B **54**, 9267 (1996).

[43] W. Luo, S. R. Nagel, T. F. Rosenbaum, and R. E. Rosensweig, Dipole Interactions with Random Anisotropy in a Frozen Ferrofluid, Phys. Rev. Lett. **67**, 2721 (1991).

[44] S. Middey, S. Ray, K. Mukherjee, P. L. Paulose, E. V. Sampathkumaran, C. Meneghini, S. D. Kaushik, V. Siruguri, K. Kovnir, and D. D. Sarma, Glasslike ordering and spatial inhomogeneity of magnetic structure in $Ba_3FeRu_2O_9$: Role of Fe/Ru site disorder, Phys. Rev. B **83**, 144419 (2011).

[45] R. S. Freitas, L. Ghivelder, F. Damay, F. Dias, and L. F. Cohen, Magnetic relaxation phenomena and cluster glass properties of $La_{0.7-x}Y_xCa_{0.3}MnO_3$ manganites, Phys. Rev. B **64**, 144404 (2001).

[46] P. M. Shand, A. L. Meyer, M. Streicher, A. Wilson, T. Rash, M. W. Roth, T. E. Kidd, and L. H. Strauss, Coulomb-driven cluster-glass behavior in Mn-intercalated $Ti_{1+y}S_2$, Phys. Rev. B **85**, 144432 (2012).

[47] R. Mathieu, P. Jönsson, D. N. H. Nam, and P. Nordblad, Memory and superposition in a spin glass, Phys. Rev. B **63**, 092401 (2001).

[48] J. Kumar, S. N. Panja, S. Dengre, and S. Nair, Identification of a Griffiths singularity in a geometrically frustrated antiferromagnet, Phys. Rev. B **95**, 054401 (2017).

[49] C. Garg, A. Cervellino, and S. Nair, Frustration, strain and phase co-existence in the mixed valent hexagonal iridate $Ba_3NaIr_2O_9$, J. Phys.: Condens. Matter **34**, 285602 (2022).

[50] J. A. Mydosh, *Spin Glasses: An Experimental Introduction* (Taylor & Francis, London, 1993), p. 256.

[51] J. Lago, I. Živković, J. O. Piatek, P. Álvarez, D. Hüvonen, F. L. Pratt, M. Díaz, and T. Rojo, Glassy dynamics in the low-temperature inhomogeneous ferromagnetic phase of the quantum spin ice $Yb_2Sn_2O_7$, Phys. Rev. B **89**, 024421 (2014).

[52] N. Marcano, J. C. Gómez Sal, J. I. Espeso, L. Fernández Barquín, and C. Paulsen, Cluster-glass percolative scenario in Ce $Ni_{1-x}Cu_x$ studied by very low-temperature ac susceptibility and dc magnetization, Phys. Rev. B **76**, 224419 (2007).

[53] S. Harikrishnan, C. M. Naveen Kumar, H. L. Bhat, S. Elizabeth, U. K. Rößler, K. Dörr, S. Rößler, and S. Wirth, Investigations on the spin-glass state in $Dy_{0.5}Sr_{0.5}MnO_3$ single crystals through

structural, magnetic and thermal properties, J. Phys.: Condens. Matter **20**, 275234 (2008).

[54] T. Chakrabarty, A. V. Mahajan, and S. Kundu, Cluster spin glass behavior in geometrically frustrated $Zn_3V_3O_8$, J. Phys.: Condens. Matter **26**, 405601 (2014).

[55] M. K. Warshi, A. Kumar, A. Sati, S. Thota, K. Mukherjee, A. Sagdeo, and P. R. Sagdeo, Cluster glass behavior in orthorhombic $SmFeO_3$ perovskite: Interplay between spin ordering and lattice dynamics, Chem. Mater. **32**, 1250 (2020).

[56] J. Alonso, M. L. Fdez-Gubieda, J. M. Barandiarán, A. Svalov, L. Fernández Barquín, D. Alba Venero, and I. Orue, Crossover from superspin glass to superferromagnet in Fe_xAg_{100-x} nanostructured thin films ($20 \leqslant x \leqslant 50$), Phys. Rev. B **82**, 054406 (2010).

[57] E. Vincent, F. Bert, J.-P. Bouchaud, V. Dupuis, J. Hammann, D. Hérisson, F. Ladieu, M. Ocio, and D. Parker, Ageing, rejuvenation and memory: The example of spin-glasses, Lect. Notes Phys. **716**, 7 (2007).

[58] A. Nag, S. Middey, S. Bhowal, S. K. Panda, R. Mathieu, J. C. Orain, F. Bert, P. Mendels, P. G. Freeman, M. Mansson, H. M. Ronnow, M. Telling, P. K. Biswas, D. Sheptyakov, S. D. Kaushik, V. Siruguri, C. Meneghini, D. D. Sarma, I. Dasgupta, and S. Ray, Origin of the Spin-Orbital Liquid State in a Nearly $J = 0$ Iridate $Ba_3ZnIr_2O_9$, Phys. Rev. Lett. **116**, 097205 (2016).

[59] H. D. Zhou, E. S. Choi, G. Li, L. Balicas, C. R. Wiebe, Y. Qiu, J. R. D. Copley, and J. S. Gardner, Spin Liquid State in the $S = 1/2$ Triangular Lattice $Ba_3CuSb_2O_9$, Phys. Rev. Lett. **106**, 147204 (2011).

[60] A. Banerjee, R. Rawat, K. Mukherjee, and P. Chaddah, Excess specific heat and evidence of zero-point entropy in magnetic glassy state of half-doped manganites, Phys. Rev. B **79**, 212403 (2009).

[61] V. Hardy, A. Maignan, S. Hébert, and C. Martin, Calorimetric and magnetic investigations of the metamagnet $Pr_{0.5}Ca_{0.5}Mn_{0.95}Ga_{0.05}O_3$, Phys. Rev. B **67**, 024401 (2003).

[62] W. Prellier, V. Smolyaninova, A. Biswas, C. Galley, R. Greene, W. Prellier, K. Ramesha, and J. Gopalakrishnan, Properties of the ferrimagnetic double-perovskites $(Ba/Ca)_2FeReO_6$, J. Phys.: Condens. Matter **12**, 965 (2000).

[63] C. Garg, D. Roy, M. Lonsky, P. Manuel, A. Cervellino, J. Müller, M. Kabir, and S. Nair, Evolution of the structural, magnetic, and electronic properties of the triple perovskite $Ba_3CoIr_2O_9$, Phys. Rev. B **103**, 014437 (2021).

[64] K. Naveen, M. Reehuis, P. Adler, P. Pattison, A. Hoser, T. K. Mandal, U. Arjun, P. K. Mukharjee, R. Nath, C. Felser, and A. K. Paul, Reentrant magnetism at the borderline between long-range antiferromagnetic order and spin-glass behavior in the *B*-site disordered perovskite system $Ca_{2-x}Sr_xFeRuO_6$, Phys. Rev. B **98**, 224423 (2018).

[65] S. Kumar, S. K. Panda, M. M. Patidar, S. K. Ojha, P. Mandal, G. Das, J. W. Freeland, V. Ganesan, P. J. Baker, and S. Middey, Spin-liquid behavior of the three-dimensional magnetic system $Ba_3NiIr_2O_9$ with $S = 1$, Phys. Rev. B **103**, 184405 (2021).

[66] I. S. Suzuki and M. Suzuki, Stretched-exponential relaxation in the three-dimensional short-range Ising spin-glass $Cu_{0.5}Co_{0.5}Cl_2$-$FeCl_3$ graphite bi-intercalation compound, Phys. Rev. B **78**, 214404 (2008).

[67] L. Lundgren, P. Svedlindh, P. Nordblad, and O. Beckman, CuMn: Dynamics of the Relaxation-Time Spectrum in Spin-Glass, Phys. Rev. Lett. **51**, 911 (1983).

[68] Y. G. Joh, R. Orbach, G. G. Wood, J. Hammann, and E. Vincent, Extraction of the Spin Glass Correlation Length, Phys. Rev. Lett. **82**, 438 (1999).

[69] E. Vincent, J. P. Bouchaud, D. S. Dean, and J. Hammann, Aging in spin glasses as a random walk: Effect of a magnetic field, Phys. Rev. B **52**, 1050 (1995).

[70] G. Kotliar and H. Sompolinsky, Phase Transition in a Dzyaloshinsky-Moriya Spin-Glass, Phys. Rev. Lett. **53**, 1751 (1984).

[71] J. R. L. de Almeida and D. J. Thouless, Stability of the Sherrington-Kirkpatrick solution of a spin glass model, J. Phys. A: Math. Gen. **11**, 983 (1978).

[72] M. Gabay and G. Toulouse, Coexistence of Spin-Glass and Ferromagnetic Orderings, Phys. Rev. Lett. **47**, 201 (1981).

[73] A. Wills, A new protocol for the determination of magnetic structures using simulated annealing and representational analysis (SARAh), Physica B: Condens. Matter **276-278**, 680 (2000).

[74] A. Wills, Indexing magnetic structures and crystallographic distortions from powder diffraction: Brillouin zone indexing, in *11th European Powder Diffraction Conference, Warsaw, September 19-22, 2008*, Vol. 30 (Walter de Gruyter GmbH & Co KG, Berlin, 2015), pp. 39–44.

[75] T. Saha-Dasgupta and D. D. Sarma, *Ab initio* study of disorder effects on the electronic and magnetic structure of Sr_2FeMoO_6, Phys. Rev. B **64**, 064408 (2001).